

The Rapid Dye Regeneration Mechanism of Dye-Sensitized Solar Cells

Jiwon Jeon,^a Young Choon Park,^b Sang Soo Han,^c William A. Goddard III,^d Yoon Sup Lee,^b and Hyungjun Kim^{*a}

Supporting Information

Section 1: Figures

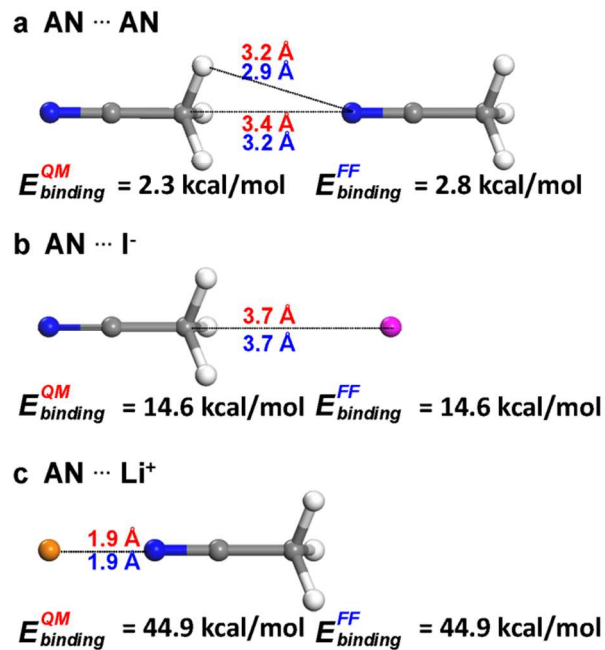


Figure S1. Comparison of geometries and binding energies from quantum mechanics (QM) in red and our DSSC-force field (QMFF-DSSC) in blue (a) Acetonitrile (AN)···acetonitrile (AN) interaction, (b) AN···I⁻ interaction, and (c) AN···Li⁺ interaction are shown. We performed QM calculation using the B3LYP exchange-correlation (xc) functional with the LACVP++ basis set, as implemented in Jaguar 7.9.¹**

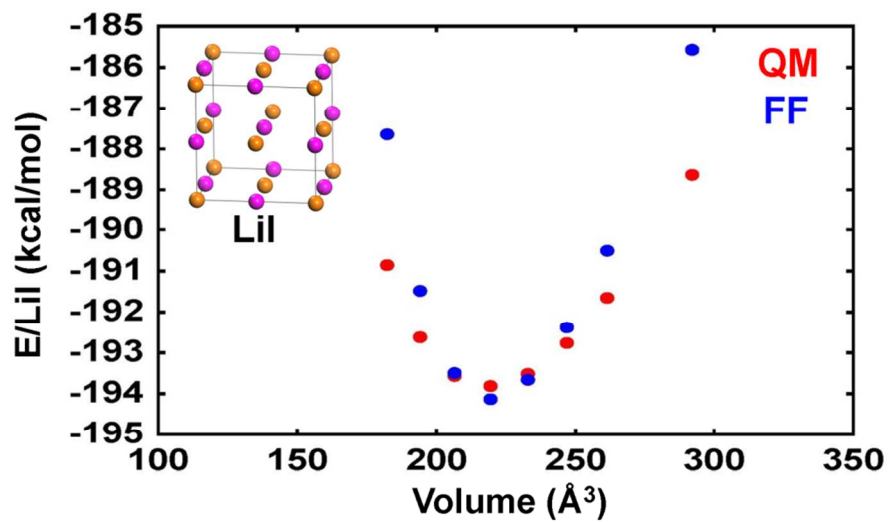


Figure S2. Equation of state (EoS) of LiI from quantum mechanics (QM) calculations in red, and EoS calculated from our DSSC-force field (QMFF-DSSC) in blue Inset shows the LiI structure (cell parameters : $6.03 \text{\AA} \times 6.03 \text{\AA} \times 6.03 \text{\AA}$). QM calculation is performed using the PBE xc-functional with the plane-wave basis set, as implemented in the Vienna Ab-initio Simulation Package (VASP).²

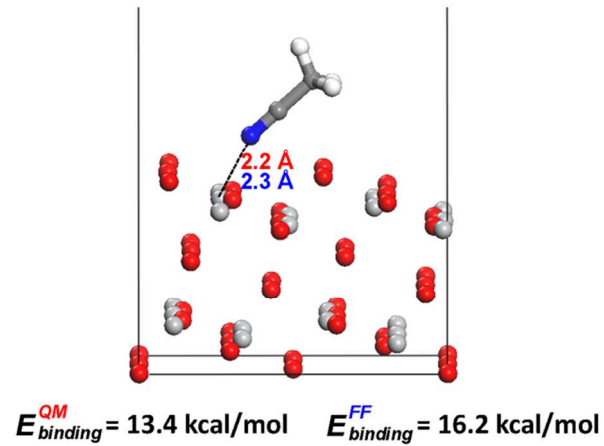


Figure S3. Comparison of geometries and binding energies from quantum mechanics (QM) in red and our DSSC-force field (QMFF-DSSC) in blue for the acetonitrile (AN)–TiO₂ surface interaction. QM calculation is performed using the PBE xc-functional with the plane-wave basis set, as implemented in the Vienna Ab-initio Simulation Package (VASP).²

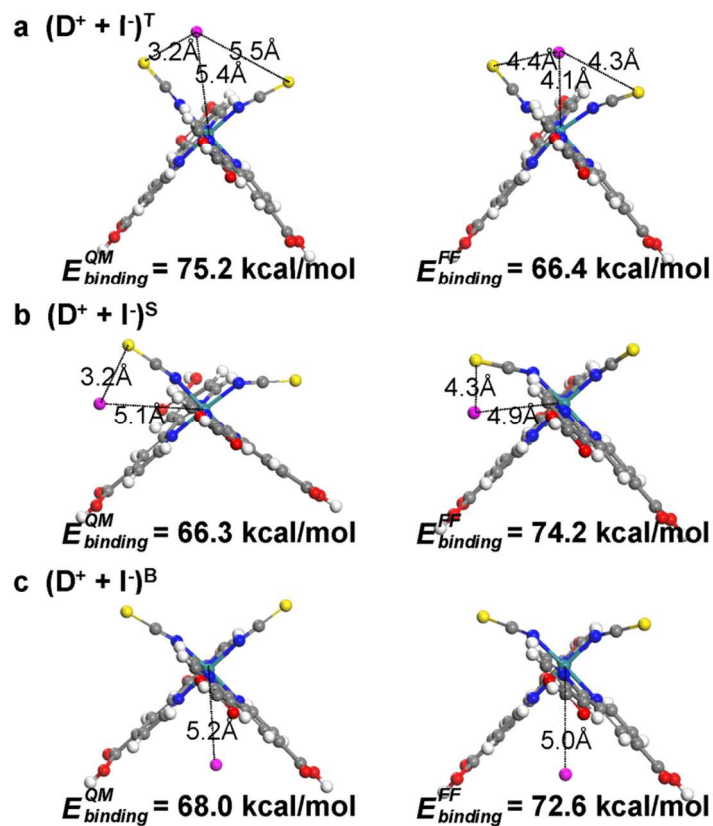


Figure S4. Comparisons of geometries and binding energies from quantum mechanics (QM) in left panels and our DSSC-force field (QMFF-DSSC) in right panels for dye (D⁺)...iodide (I⁻) interactions (a) (D⁺+I⁻)^T orientation, (b) (D⁺+I⁻)^S orientation, and (c) (D⁺+I⁻)^B orientation are shown. QM calculation were performed using the B3LYP exchange-correlation (xc) functional with the LACVP** basis set, as implemented in Jaguar 7.9.¹

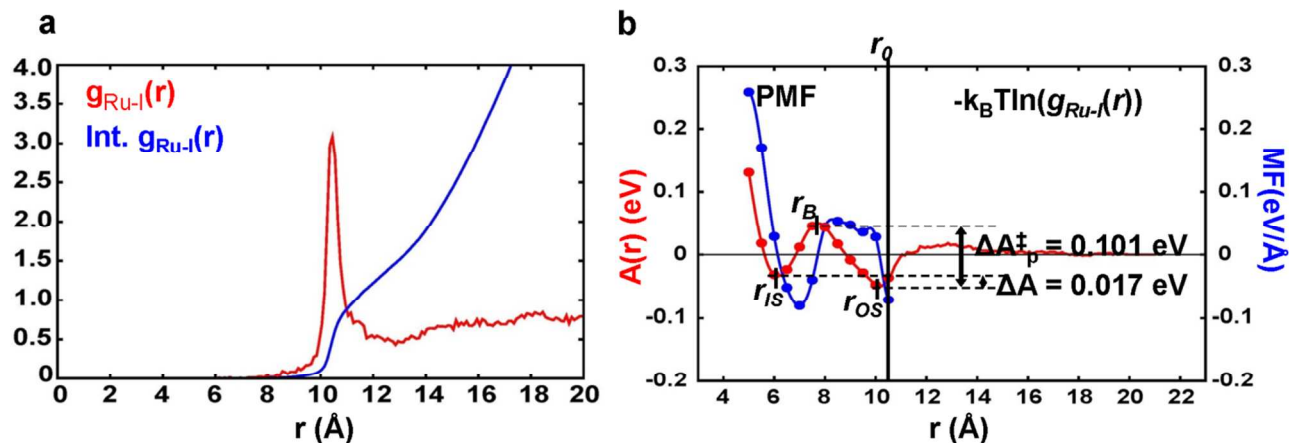


Figure S5. (a) The radial distribution function (RDF) of Ru and I, $g_{Ru-I}(r)$, from last 10 ns of the NVT MD simulations with the sideways dye configuration. The peak is at 10.5 Å and the minimum position is ~12.5 Å. The coordination number (CN) is 1.3 at this minimum position. (b) Calculated free energy profile, $A(r)$, as a function of the Ru...I distance (r) for the case of the sideways configuration. For the regime where the sampling quality of the radial distribution function between Ru and I is high [$r > 10.5$ Å], we computed $A(r)$ by directly converting $g_{Ru-I}(r)$. When $r < 10.5$ Å, we intensively sampled the penetration events by using constrained MD simulations. From a series of MD simulations performed while constraining r , we obtained the r -dependent mean force (MF) profile, which is shown as a blue dotted curve, the integration of which led to the potential of mean force (PMF), which is equivalent to the free energy profile. The free energy profile of sideways configuration is quantitatively similar with that of upright configuration (see Figure 4), which implies that the RDFs of both upright and sideways configurations should be ideally similar to each other. However, due to the incompleteness of sampling the penetration events over the finite MD time scale, the RDF for the sideways configuration calculated using the conventional MD simulation does not have the peak at the inner-sphere regime ($r \sim 6.0$ Å). The energy barrier for the penetration of I, ΔA_p^\ddagger , was determined to be 0.101 eV, leading to a rate constant for penetration (k_p) of $2.3 \times 10^{11} \text{ s}^{-1}$ and a time scale of ~ 4 ps.

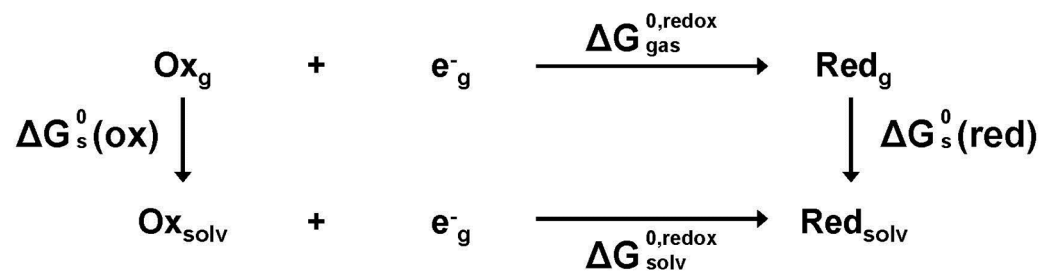


Figure S6. Born-Harbor cycle used to calculate the reduction potentials of iodide and dye.

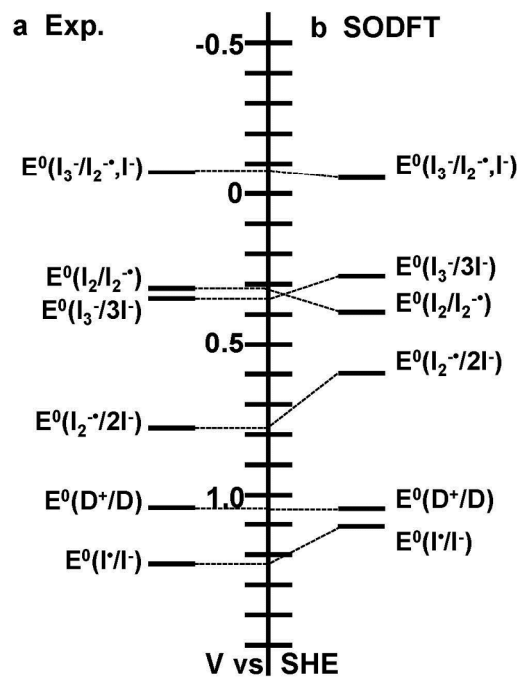


Figure S7. Standard reduction potentials (E^0). (a) Experimental values³⁻⁶ are compared with (b) DFT results taken from our previous work.⁷ We used B3LYP with aug-cc-pVTZ-pp coupled with Poisson-Boltzmann implicit solvation (PBIS) using Jaguar¹, and then carried out spin-orbit correction using spin-orbit DFT (SODFT) with B3LYP method as implemented in NWChem package.⁸

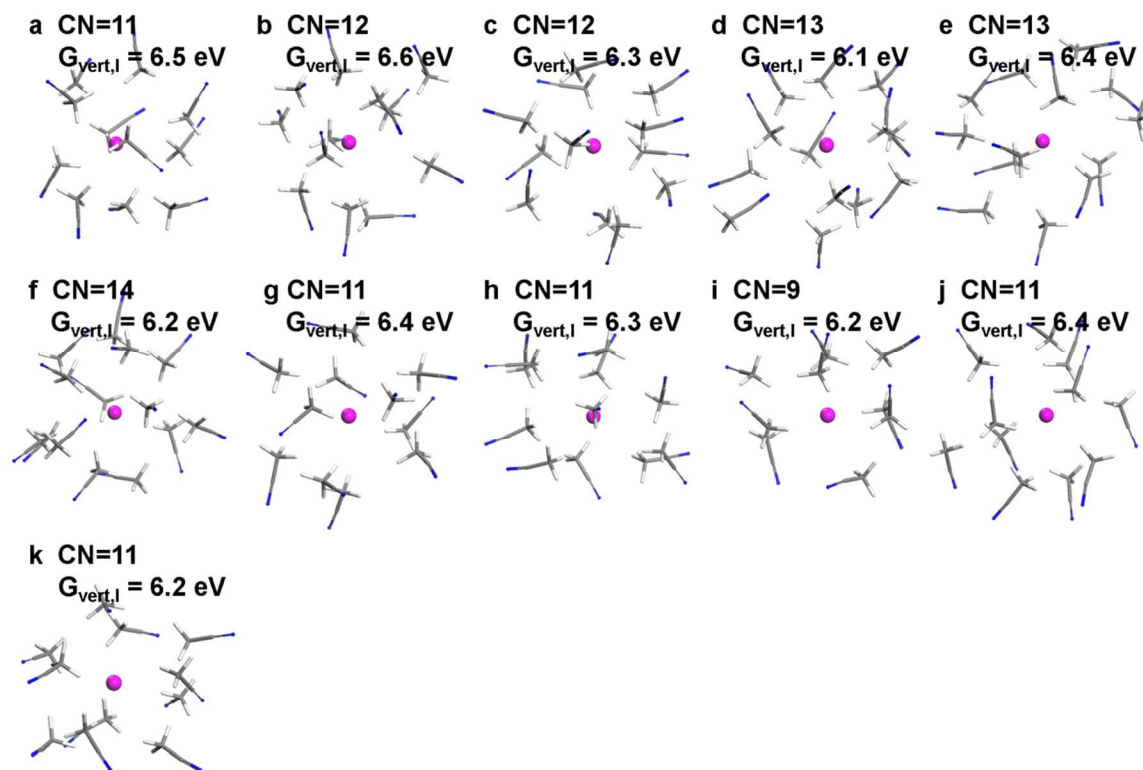


Figure S8. 11 sampled acetonitrile solvation shell of I^- from last 1ns MD in 2ns NVT simulation of bulk system. The vertical excitation energy ($G_{vert,I}$) of each structure are presented as well as the coordination number (CN) of I^- . We obtained 11 snapshots (with a time interval of 100 ps) from the last 1 ns of the 2 ns NVT MD simulations of the bulk electrolyte phased system consisting of 35 Li^+ , 5 I_3^- and 30 I^- dissolved in 957 acetonitrile (AN) molecules. By tagging one iodide, we sampled 11 different cases for iodides surrounded by first solvation shell structures. (a-k) The average $G_{vert,I}$ (without spin-orbit effect correction) is 6.328 eV and the average CN is 11.6 (cf. the CN averaged over all 30 iodides for 2,000 snapshots is 11.3).

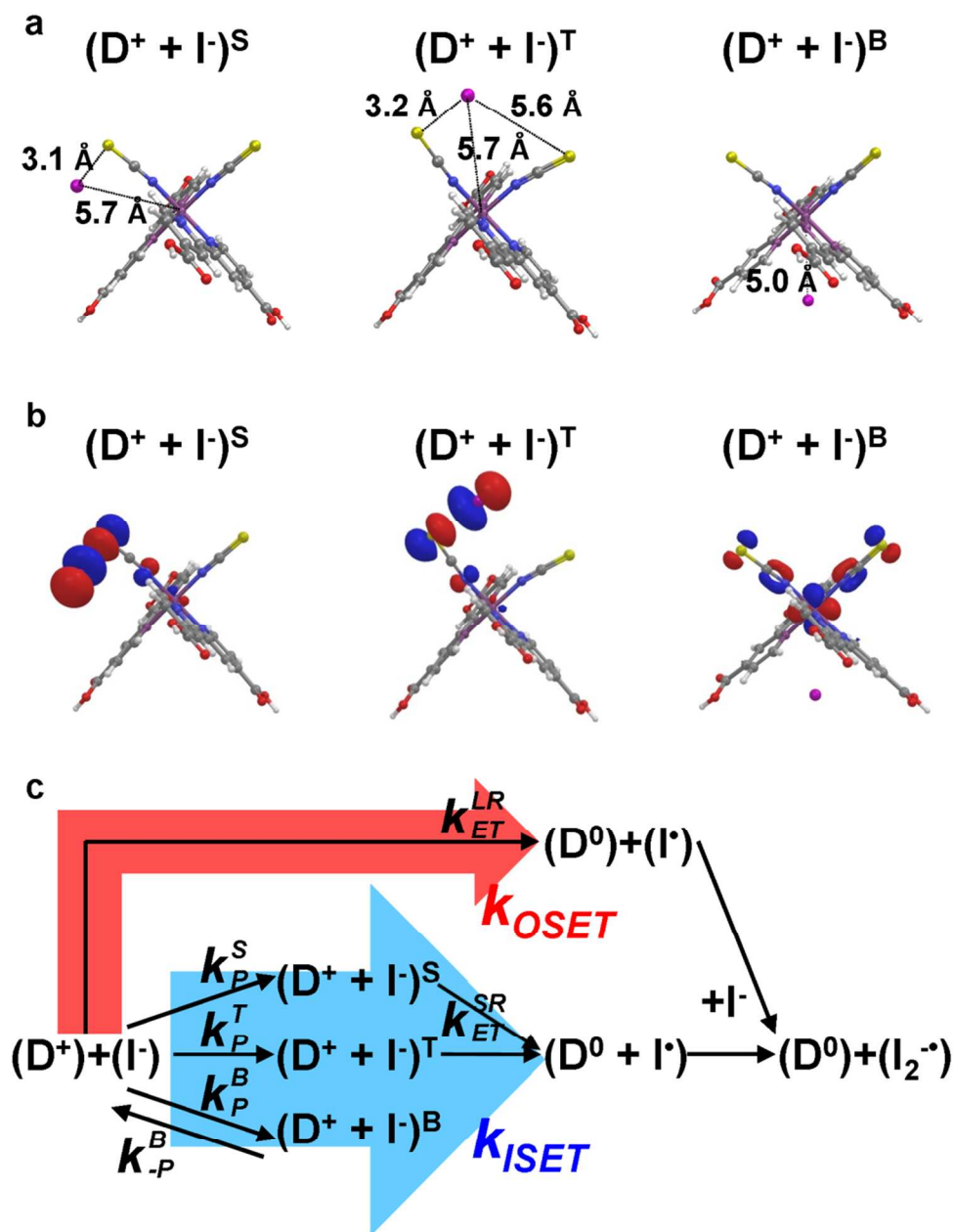


Figure S9. Atomistic structures and singly occupied molecular orbital (SOMO) of $(D^+ + I^-)$ depending on the orientation of I^- with respect to D^+ . Scheme showing the three dye regeneration pathways (a) $(D^+ + I^-)^S$ denotes that I^- is located between the NCS ligand and the 4,4'-dicarboxy-2,2'-bipyridine (*dcb*) ligand. $(D^+ + I^-)^T$ denotes that I^- is located between two NCS ligands. $(D^+ + I^-)^B$ denotes that I^- is located between two *dcb* ligands of D^+ . (b) SOMO of three different orientations, $(D^+ + I^-)^S$, $(D^+ + I^-)^T$, and $(D^+ + I^-)^B$, obtained from density functional theory (DFT) calculations. This figure shows that the immediate charge delocalization of I^- to D^+ occurs only in the $(D^+ + I^-)^S$ and $(D^+ + I^-)^T$ orientations, implying that the fast short-range ET is only available via the aid of NCS ligands (the Mulliken spin density of I^- is 0.55 for $(D^+ + I^-)^S$ and 0.60 for $(D^+ + I^-)^T$, while the Mulliken spin density of I^- for $(D^+ + I^-)^B$ is only 0.03). (c) D^+ and D^0 denote the oxidized and neutralized dye molecules, respectively, while I^- and I^* denote the iodide and iodine atoms, respectively. The parenthesis represents the solvation shell, i.e., $(D^+) + (I^-)$ indicates that the solvation shell of each of D^+ and I^- is separately developed, while $(D^+ + I^-)$ indicates that both D^+ and I^- are located within the same solvation shell. Depending on the nature of the electron transfer (ET), we consider two extreme pathways: 1) the electron of I^- is transferred directly to D^+ across the solvation shell boundary over

a long range ($> 10 \text{ \AA}$), i.e., the outer-sphere electron transfer (OSET) pathway (shown in red); 2) the I^- partially loses its solvation shell, while penetrating to a location close to the D^+ molecule, and then transfers an electron through direct orbital-orbital interactions, i.e., the inner-sphere electron transfer (ISET) pathway (shown in blue).

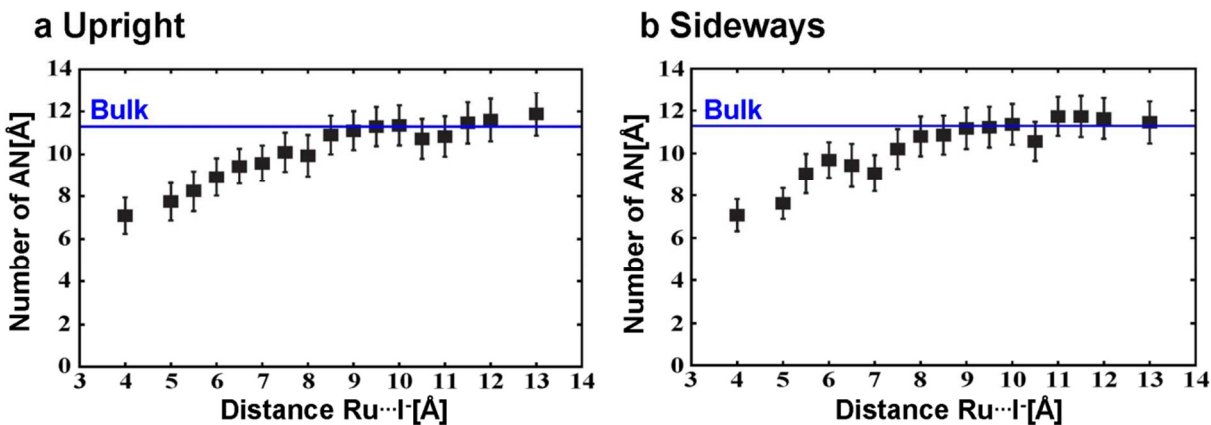


Figure S10 Number of acetonitrile (AN) around Γ^- from constrained molecular dynamic (MD) simulation as a function of $\text{Ru}\cdots\Gamma^-$ distance in (a) 'upright' (b) 'sideways' configuration. We examined the first coordination number (CN) of Γ^- with AN depends on the separation (distance $\text{Ru}\cdots\Gamma^-$, defined as r). The cutoff distance between Γ^- and carbon atom of methyl group of AN is 6.0 Å. To compare the bulk property, we analyze 2,000 snapshots from the NVT of bulk system. In bulk system, the number of AN around Γ^- is 11.3. (blue) When $r > \sim 10$ Å, we found that the first CN converges to the bulk value of 11.3. This result supports the view that the Γ^- at a distance of ~ 10 Å from Ru is fully solvated in a manner similar to that of the bulk phase, while at a distance of ~ 6 Å of the Γ^- from Ru has lost 18% of its own solvation shell to merge the solvation shells of Γ^- and D^+ .

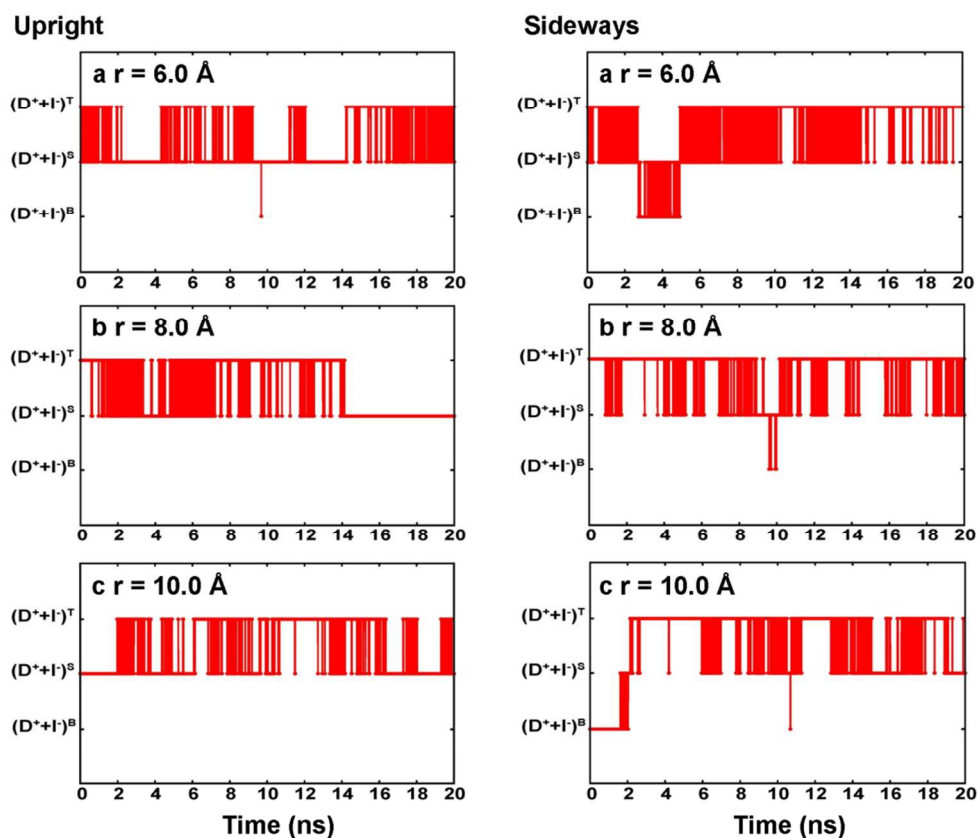


Figure S11. Orientations of Γ with respect to D^+ sampled from constrained MD simulations at the distance between Ru and Γ (r) is (a) 6.0 \AA , (b) 8.0 \AA , and (c) 10.0 \AA . For upright configuration (left panels), Γ travels between top site $[(D^++\Gamma)^T]$ and side site $[(D^++\Gamma)^S]$ frequently, but no visit to the bottom site $[(D^++\Gamma)^B]$ since the bottom site is blocked with TiO_2 surface. For sideways configuration (right panels), Γ travels among top site $[(D^++\Gamma)^T]$, side site $[(D^++\Gamma)^S]$, and bottom site $[(D^++\Gamma)^B]$ frequently.

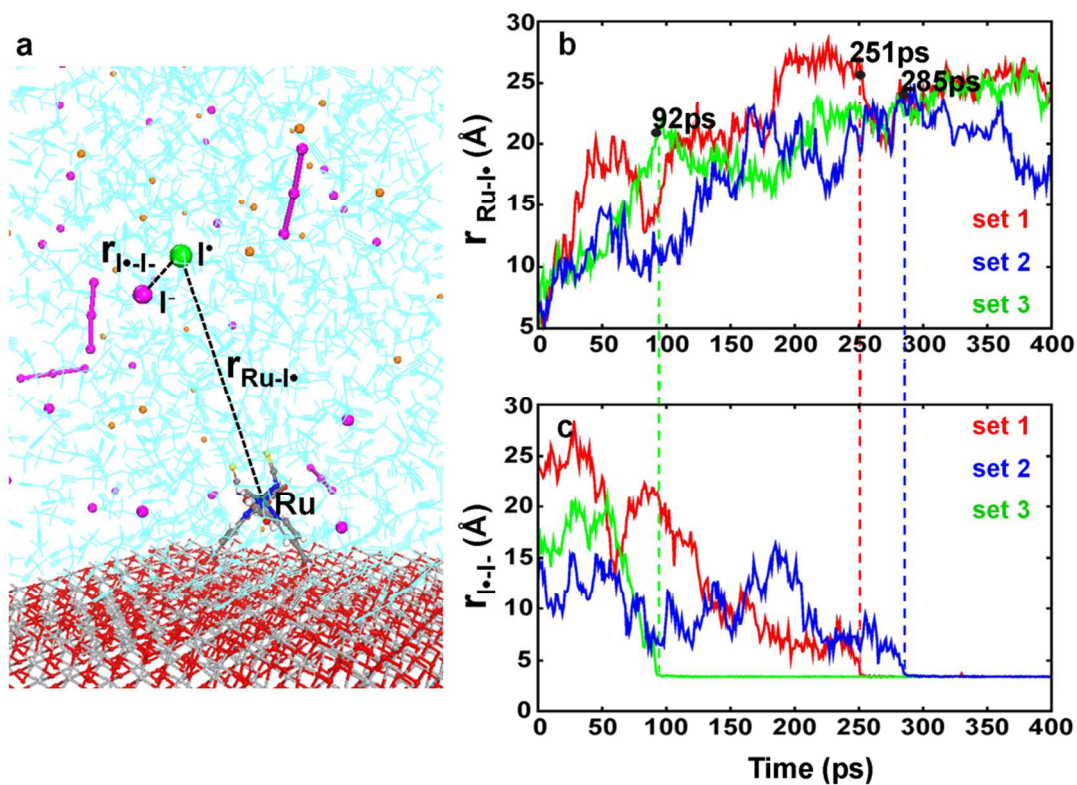


Figure S12. I-I bond formation after the ISET process. With I^- is located at the inner-sphere position ($\sim 6 \text{ \AA}$), we instantaneously changed the charge distribution of the dye molecule from D^+ to D^0 while converting the I^- to I^\bullet to mimic the ET in our classical MD simulation. We used a Morse potential to describe the pair potential between I^- and I^\bullet , the parameters of which were optimized to reproduce the bond energy and vibrational frequency of I_2^\bullet . We then continued MD simulation. (a) snapshot of MD simulation. From three independent MD simulation sets, we found that (b) I^\bullet diffuses away from D^0 until a distance of 20-25 \AA from the Ru center whereupon (c) I_2^\bullet forms by colliding with another I^- at 251 ps (simulation set 1), 285 ps (simulation set 2), and 92 ps (simulation set 3).

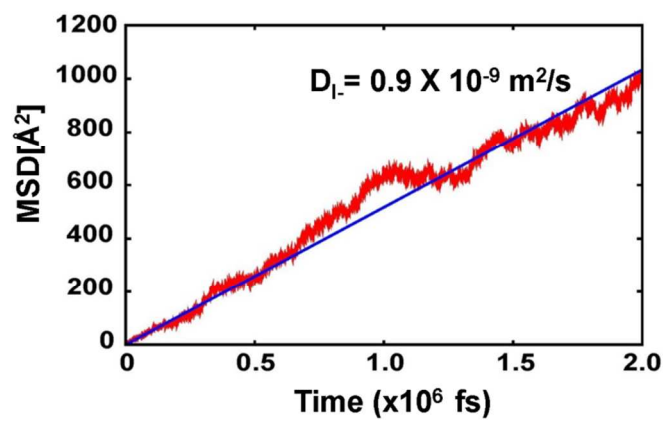


Figure S13. Mean-squared displacement of Γ in acetone solution Diffusion constant of Γ (D_l) from 2ns NVT of bulk system is calculated as $0.9 \times 10^{-9} \text{ m}^2/\text{s}$. The experiment value of D_l is $1.7 \times 10^{-9} \text{ m}^2/\text{s}$.⁹

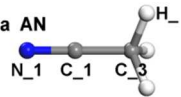
Section 2: Tables

	Upright		Sideways		Short range ET
	$\Delta A_p^{\ddagger, o}$ [eV]	k_p^o [ps ⁻¹]	$\Delta A_p^{\ddagger, o}$ [eV]	k_p^o [ps ⁻¹]	
$(D^+ + I)^S$	0.099	0.13	0.102	0.06	Available
$(D^+ + I)^T$	0.097	0.12	0.096	0.17	Available
$(D^+ + I)^B$	$\gg k_B T$	~ 0	0.249	1.4×10^{-4}	Not available


Table S1. Orientation-dependent free energy barriers for I^- penetration, $\Delta A_p^{\ddagger, o}$ for the orientations where the short range electron transfer is available [$(D^+ + I)^S$ and $(D^+ + I)^T$] and where the short range electron transfer is not available [$(D^+ + I)^B$]. Using transition state theory, the rate constants of k_p^o were calculated.

VdW on diagonal term	$R_0[\text{\AA}]$	$D_0[\text{kcal/mol}]$
Li^+	0.03	2.45
$\text{I}(\text{I}^-, \text{I}^+, \text{I}_3^-)$	0.34	4.50
N 1	0.08	3.66
C 1	0.10	3.90
C 3	0.10	3.90
H	0.02	3.20
C RD	0.10	3.90
N RD	0.08	3.66
N 2D	0.08	3.66
S 3D	0.34	4.03
O 2D	0.10	3.40
O RD	0.10	3.40
H D	0.02	3.20
H AD	0.00	3.10
Ru D	0.06	2.96
C 1D	0.10	3.90


a AN



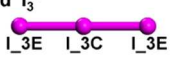
b Li^+



c I^-



d I_3^-



e D^+

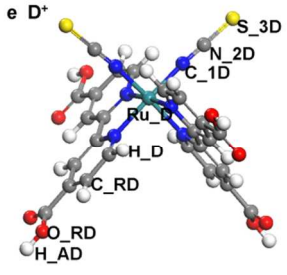


Table S2. Atom types and van der Waals force field (FF) parameters Van der Waals (vdW) on diagonal terms were from DREIDING FF¹⁰ with the 12-6 Lennard-Jones functional form: $E_{LJ12-6} = D_0 \left\{ \left(\frac{R_0}{r} \right)^{12} - 2 \left(\frac{R}{r} \right)^6 \right\}$. We show atom types of (a) acetonitrile (AN), (b) Li^+ , (c) I^- , (d) I_3^- , and (e) dye molecule (D^+).

VdW on diagonal term	A[kcal/mol]	B [Å]	C[kcal/mol·Å⁶]
Ti-Ti	716944.16	6.50	120.83
O-O	271449.87	4.27	696.18
VdW off diagonal term	A[kcal/mol]	B [Å]	C[kcal/mol·Å⁶]
Ti-O	390665.92	5.16	289.86
Ti-O_RD	390665.92	5.16	289.86

Table S3. Force field parameters for TiO₂ Buckingham potential is employed to use the classical Born model for TiO₂¹¹: $E_{TiO_2} = A \exp(-Br) - \frac{C}{r^6}$. The chemisorption of the dye molecule to the TiO₂ surface (interaction between O_RD in dye molecule and Ti of TiO₂) is described by using the same parameter of Ti-O interaction for TiO₂.

VdW off diagonal term	$R_0[\text{\AA}]$	$D_0[\text{kcal/mol}]$
N_1···I-	3.90	0.20
C_3···I-	3.55	0.05
H···I-	3.66	1.26
N_1···Li+	2.00	9.73
C_3···Li+	2.35	9.50
H···Li+	2.20	0.50
N_1···H	3.00	0.00

Table S4. Off-diagonal van der Waals (vdW) force field parameters Off diagonal vdW parameters were optimized for the accurate interaction of AN···I⁻, AN···Li⁺ and AN···AN. The other off-diagonal vdW parameters not listed in this table was derived from the geometric mean of on-diagonal vdW parameters.

VdW off diagonal term	D ₀ [kcal/mol]	R ₀ [Å]	y
Li ⁺ ...I	1.20	3.54	12.00

Table S5. Force field parameters for LiI The interaction between Li⁺ and I were optimized to reproduce the equation of states of LiI using Morse potential: $E_x = D_0 \left\{ \frac{y}{y-6} \exp \left(y \left(1 - \frac{r}{R_0} \right) \right) - \frac{y}{y-6} \left(\frac{R_0}{r} \right)^6 \right\}$.

VdW off diagonal term	D ₀ [kcal/mol]	r ₀ [Å]	y
Γ···Γ	32.71	3.46	53.87

Table S6. Force field parameters for the interaction of Γ and I[•] The chemical bond of I₂[•] is described using Morse potential: $E_x = D_0 \left\{ \frac{y}{y-6} \exp \left(y \left(1 - \frac{r}{R_0} \right) \right) - \frac{y}{y-6} \left(\frac{R_0}{r} \right)^6 \right\}$. This leads to the bond distance of 3.46 Å, bond dissociation energy of 32.71 kcal/mol, and vibration frequency of 86.11 cm⁻¹ in consistent with the DFT results calculated using B3LYP and LACVP**++ basis set.

Section 3: Computational details

1. Modeling of the TiO₂-dye-electrolyte interface.

We model the photoanode of dye-sensitized solar cells (DSSCs) as a TiO₂-dye-electrolyte interface as shown in Figure 1; the model consists of

- a 39.09 Å × 39.13 Å (101) surface of anatase TiO₂ with 2 bilayers, but the bottom layer fixed,
- the N3 dye, which has the chemical formula of *cis*-[Ru^{II}(*dcb*)₂(NCS)₂] (*dcb* = 4,4'-dicarboxy-2,2'-bipyridine), and
- an acetonitrile (AN)-based electrolyte with ionic salts.⁴

The AN electrolyte phase contains 30 I⁻, 5 I₃⁻, and 34 Li⁺ together with 957 AN molecules, which is equivalent to 0.6 M I⁻, 0.1 M I₃⁻, and 0.7 M Li⁺ in AN, respectively. The AN electrolyte phase modelled here represent conditions where 0.7 M LiI and 0.1 M I₂ are dissolved in AN under the assumption that all I₂ is converted into I₃⁻ by consuming equimolar I⁻, which is similar to the conventional experimental conditions.^{12,13} The charge neutrality of the cell is satisfied by including a single oxidized dye (D⁺).

The dye molecule (D) is tethered to the TiO₂ surface by anchoring the carboxylic groups to the 5-coordinated Ti atoms. The ATR-FTIR spectrum analysis indicated that two anchors among four carboxylates of the N3 dye participate in the adsorption of the dye onto the TiO₂ surface.^{14,15} Therefore, we consider two possible configuration of the dye molecule on the TiO₂ surface, 'upright' and 'sideways' configurations, as shown in Figure 1. For the 'upright' configuration, the dye molecule is adsorbed onto the TiO₂ surface via two carboxyl groups from different *dcb* ligands. Here, the dipole moment of the dye molecule is aligned to be nearly perpendicular to the TiO₂ surface. For the 'sideways' configuration, the dye molecule is adsorbed onto the TiO₂ surface via two carboxyl groups from the same *dcb* ligands. This configuration causes the direction of the dipole moment of the dye molecule to be almost parallel to the TiO₂ surface.

Considering that the N3 dye molecule has *pK_a* values of 3.0 and 1.5,¹⁶ we doubly deprotonated the dye molecule, resulting in two COO⁻ groups that were used to anchor the dye molecule to the 5-coordinated Ti atoms of the TiO₂ surface. Two protons separated from the dye molecule were attached to the adjacent oxygen atoms of the TiO₂ surface (Figure 1).

2. First-principles-based force field parameters.

To accurately describe the energetics of the TiO₂-dye-electrolyte interface, where inorganic, organometallic, and organic species coexist, we used the following combination of force fields (FFs): the classical Born model for TiO₂,¹¹ the universal force field (UFF)¹⁷ for the organometallic dye molecule, and the DREIDING FF¹⁰ for the organic electrolyte system. We then optimized the combined FFs to reproduce the QM nonbonded interaction energies (van der Waals attraction and coulombic). We refer to this newly developed first-principles-based FF as QMFF-DSSC. The full details of the parameters of the QMFF-DSSC are summarized in Table S2-6.

Note that the QMFF-DSSC model reproduces the QM DFT results in terms of the structures and energetics for the following important interactions:

- AN-AN interactions (Figure S1a),
- AN-I⁻ interactions (Figure S1b),
- AN-Li⁺ interactions (Figure S1c),
- Li⁺-I⁻ interactions (reproducing the equation-of-state of the LiI crystal; Figure S2),
- AN-TiO₂ surface interactions (Figure S3), and
- D⁺-I⁻ interactions (Figure S4).

The DFT calculations used for the training of QMFF-DSSC were performed using the B3LYP exchange-correlation (xc) functional with the LACVP** basis set, as implemented in Jaguar 7.9,¹ or using the PBE xc-functional with the plane-wave basis set, as implemented in the Vienna Ab-initio Simulation Package (VASP).²

3. Molecular dynamics (MD) simulation procedures.

Using QMFF-DSSC, we performed MD simulations at 340 K and 1 atm with the 2 bottom bilayers of TiO₂ fixed and the other two flexible. We used the Large-scale Atomic/Molecular Massively Parallel Simulator (LAMMPS), with the following MD procedure:

- 1) Three-nanosecond isobaric-isothermal (NPT) MD simulations at 340 K (Nosé-Hoover thermostat with a damping constant of 0.1 ps) and 1 atm (Andersen barostat with a damping constant of 2 ps), allowing for the volume change only along the z-axis, which is the normal direction to the TiO₂ surface,
- 2) Calculation of the converged simulation cell volume, which is determined as 39.09 Å × 39.13 Å × 64.42 Å,
- 3) Isothermal (NVT) MD simulations at 340 K over 20 ns, where the last 10 ns of trajectories were used for the analysis.

For the constrained MD simulations used for computation of the potential of mean force, we performed 12 sets of constrained MD simulations with various Ru···I distances over the range of 5 Å to 10.5 Å. For each simulation set, the Ru···I distance was constrained by implementing Gauss' least constraints principle¹⁸ in our local LAMMPS program. The modified equations of motions for Ru and I atoms under the constraints are

$$m_{Ru}\ddot{r}_{Ru} = F_{Ru} - \Lambda r \quad (1)$$

$$m_I\ddot{r}_I = F_I + \Lambda r \quad (2)$$

where the multiplier, " Λ ", is given as

$$\Lambda = -\frac{r(m_{Ru}F_I - m_I F_{Ru}) + m_{Ru}m_I\dot{r}^2}{(m_{Ru} + m_I)r^2}. \quad (3)$$

We performed 31 ns of constrained MD simulations at 340 K and 1 atm for each distance, during which the constraining force was sampled every 10 fs during the last 10 ns, leading to 10⁶ mean force data points.

4. Density functional theory (DFT) calculations.

To calculate the reorganization energies and the standard reduction potentials, we performed DFT calculations coupled with the Poisson Boltzmann Implicit Solvation (PBIS) method using Jaugar 7.9.¹ We used the B3LYP xc-functional coupled with the LACVP**++ basis set for describing acetonitrile (AN) and LACVP** basis set for the dye molecule, whereas the more extensive basis set cc-pvtz-pp++ was used for the iodine species I⁻ and I[•]. The standard reduction potentials were calculated using the Born-Harbor cycle, as shown in Figure S6.

Since, iodine radical has a considerable spin-orbit coupling (SOC), we performed spin-orbit DFT (SODFT) calculations using the NWChem software⁸ with the B3LYP xc-functional and the aug-cc-pVTZ-pp basis set. This was used to correct for the SOC effect.

Section 4: Mathematical details

1. Mathematical details for the free energy profile, $A(r)$

We defined the reaction coordinate of our system as the distance (r) between the Γ and the Ru center of D^+ , and we computed the potential of the mean force (PMF), i.e., the free energy profile along the reaction coordinate, $A(r)$, by integrating the mean force (MF) along the reaction coordinate, $-dA(r)/dr$ ¹⁹:

$$A(r) - A(r_0) = \int_{r_0}^r \frac{dA(r')}{dr'} dr' \quad (4)$$

Here, $A(r_0)$ is the free energy at the reference point $r = r_0$, and MF is a measurable quantity from our constrained MD simulations.

The change of MF as a function of r is shown in Figure 4, and its integration from $r = r_0$ to the given r [equation (4)] provides $A(r) - A(r_0)$, which is the profile of the relative free energy with respect to $A(r_0)$ when $r < r_0$. In our calculations, we chose $r_0 = 10.5 \text{ \AA}$, near where the largest peak of $g_{Ru-I}(r)$ is positioned.

When $r > r_0$, for a sufficiently high population of $g_{Ru-I}(r)$, we can compute the free energy profile straightforwardly using $g_{Ru-I}(r)$ obtained from the unconstrained MD simulation:

$$A(r; r > r_0) = -k_B T \ln g_{Ru-I}(r) \quad (5)$$

which gives us the absolute location of $A(r_0)$ with respect to $A(\infty)$, where $A(\infty)$ is set to be zero.

Combining the free energy profile computed from $g_{Ru-I}(r)$ when $r > r_0$ and that computed from PMF when $r < r_0$, we obtained the entire free energy profile of $A(r)$ shown in Figure 4. Regardless of the dye orientation (either upright or sideways), the free energy barrier for the penetration, ΔA_p^\ddagger , was calculated as $\sim 0.1 \text{ eV}$ (0.098 eV for the upright orientation and 0.101 eV for the sideways orientation; Figure S5b).

2. Mathematical details for the orientation and distance dependent free energy barriers

Calculations of orientation dependent free energy, $A^S(r)$, $A^T(r)$, and $A^B(r)$

To mathematically define the orientation of Γ with respect to the Ru center of dye molecule without ambiguity, we considered 6 vectors connecting from the position of Ru center to the position of N atom of the ligand for the given snapshot. Depending on the N atom is from NCS ligands or *dcb* ligands, we denote the Ru-N vector either as $\mathbf{r}_{Ru-N(NCS)}$ (when the N is from the NCS ligands) or $\mathbf{r}_{Ru-N(dcb)}$ (when the N is in the *dcb* ligands). There exists two $\mathbf{r}_{Ru-N(NCS)}$'s and four $\mathbf{r}_{Ru-N(dcb)}$'s, which partitions the entire space into eight separated spaces (imagine the eight faces of the octahedron). Each space is then classified into one of the following cases;

- (case 1) the space of which boundary is defined by two $\mathbf{r}_{Ru-N(NCS)}$'s and one $\mathbf{r}_{Ru-N(dcb)}$;
- (case 2) the space of which boundary is defined by one $\mathbf{r}_{Ru-N(NCS)}$ and two $\mathbf{r}_{Ru-N(dcb)}$'s; and
- (case 3) the space of which boundary is defined by three $\mathbf{r}_{Ru-N(dcb)}$'s.

When the Γ is located in the space of case 1, it is defined as in the top site orientation, $(D^+I)^T$; when the Γ is located in the space of case 2, it is defined as in the side site orientation, $(D^+I)^S$; and when the Γ is located in the space of case 3, it is defined as in the bottom site orientation, $(D^+I)^B$.

We now consider the probability that the Γ locates at the distance of r from the Ru center and at the orientation of o that can be either one of top (T), side (S), or bottom (B), $P(r \wedge o)$. By introducing the conditional probability of a certain orientation at a given r , $P(o | r)$, we write $P(r \wedge o) = P(o | r) \cdot P(r)$.

Then, the orientation and distance dependent free energy, $A^o(r)$, becomes

$$\begin{aligned} A^o(r) &= -k_B T \ln P(r \wedge o) \\ &= -k_B T \ln P(r) - k_B T \ln P(o | r) \end{aligned}$$

$$=A(r)-k_B T \ln P(o | r)$$

where $A(r)$ is the distance dependent free energy profile shown in Figure 4 of the manuscript for the upright configuration and in Supplementary Figure S5b for sideways configuration.

By analyzing the trajectories of constrained MD simulations, we can compute the dwelling time of Γ at each orientation site (see Supplementary Figure S11), and then simply convert it to $P(o | r)$. By following this way, we computed $P(o=T | r)$, $P(o=S | r)$, and $P(o=B | r)$, at $r = r_{IS} = 6.1 \text{ \AA}$ (inner-sphere position), $r = r_B = 7.7 \text{ \AA}$ (barrier position), and $r = r_{OS} = 10.2 \text{ \AA}$ (outer-sphere position). This yields barrier heights for the penetration as $\Delta A_p^{\ddagger o} = A^o(r=r_B) - A^o(r=r_{OS})$, which are summarized in the Table S1 of the Supplementary Information.

Then, the transition state theory gives $\tilde{k}_p^o = k_B T / h \exp[-\Delta A_p^{\ddagger o} / k_B T]$, where \tilde{k}_p^o is the rate constant for the penetration of Γ from the outer-sphere position (r_{OS}) with the orientation of o . Thus the reaction rate is proportional to $\tilde{k}_p^o [\Gamma]_{r_{OS}, o}$ where $[\Gamma]_{r_{OS}, o}$ denotes the local concentration of Γ at $r = r_{OS}$ with the orientation of o . Since the concentration of Γ at $r = r_{OS}$, $[\Gamma]_{r_{OS}}$ is simply given as $P(o|r=r_{OS})[\Gamma]_{r_{OS}, o}$, the rate constant for the penetration of Γ from the outer-sphere position is given as $k_p^o = \tilde{k}_p^o P(o|r=r_{OS})$.

From this calculation, we determined that

- $\Delta A_p^{\ddagger S} = 0.099 \text{ eV}$ for the upright dye orientation and
- $\Delta A_p^{\ddagger S} = 0.102 \text{ eV}$ for the sideways dye orientation,
- $\Delta A_p^{\ddagger T} = 0.097 \text{ eV}$ for the upright dye orientation and
- $\Delta A_p^{\ddagger T} = 0.096 \text{ eV}$ for the sideways dye orientation, and
- we observed no penetration into the bottom site for the upright dye orientation because the approach of iodide to the bottom site is hindered by the TiO_2 surface (i.e., $\Delta A_p^{\ddagger B} \gg k_B T$) for the geometry considered and
- $\Delta A_p^{\ddagger B} = 0.249 \text{ eV}$ for the sideways dye orientation.

In conjunction with transition state theory (TST), these results yield the rate constants of (values are summarized in Table S1).

- $k_p^S = 1.3 \times 10^{11} \text{ s}^{-1}$ for the upright dye orientation and
- $k_p^S = 6.0 \times 10^{10} \text{ s}^{-1}$ for the sideways dye orientation,
- $k_p^T = 1.2 \times 10^{11} \text{ s}^{-1}$ for the upright dye orientation and
- $k_p^T = 1.7 \times 10^{11} \text{ s}^{-1}$ for the sideways dye orientations, and
- $k_p^B \approx 0$ for the upright dye orientation and
- $k_p^B = 1.4 \times 10^8 \text{ s}^{-1}$ for the sideways dye orientation

References

- (1) Maestro *Schrodinger, LLC, New York* **2009**.
- (2) Kresse, G.; Furthmuller, J. Efficiency of ab-initio total energy calculations for metals and semiconductors using a plane-wave basis set. *Comput. Mater. Sci.* **1996**, *6*, 15-50.
- (3) Wang, X. G.; Stanbury, D. M. Oxidation of iodide by a series of Fe(III) complexes in acetonitrile. *Inorg. Chem.* **2006**, *45*, 3415-3423.
- (4) Nazeeruddin, M. K.; Kay, A.; Rodicio, I.; Humphrybaker, R.; Muller, E.; Liska, P.; Vlachopoulos, N.; Gratzel, M. CONVERSION OF LIGHT TO ELECTRICITY BY CIS-X2BIS(2,2'-BIPYRIDYL-4,4'-DICARBOXYLATE)RUTHENIUM(II) CHARGE-TRANSFER SENSITIZERS (X = CL-, BR-, I-, CN-, AND SCN-) ON NANOCRYSTALLINE TiO₂ ELECTRODES. *J. Am. Chem. Soc.* **1993**, *115*, 6382-6390.
- (5) Boschloo, G.; Gibson, E. A.; Hagfeldt, A. Photomodulated Voltammetry of Iodide/Triiodide Redox Electrolytes and Its Relevance to Dye-Sensitized Solar Cells. *J. Phys. Chem. Lett.* **2011**, *2*, 3016-3020.
- (6) Datta, J. B., A.; Kundu, K. *Bull. Chem. Soc. Jpn.* **1988**, *61*, 1735.
- (7) Jeon, J.; Goddard, W. A.; Kim, H. Inner-Sphere Electron-Transfer Single Iodide Mechanism for Dye Regeneration in Dye-Sensitized Solar Cells. *J. Am. Chem. Soc.* **2013**, *135*, 2431-2434.
- (8) Valiev, M.; Bylaska, E. J.; Govind, N.; Kowalski, K.; Straatsma, T. P.; Van Dam, H. J. J.; Wang, D.; Nieplocha, J.; Apra, E.; Windus, T. L.; de Jong, W. NWChem: A comprehensive and scalable open-source solution for large scale molecular simulations. *Comput. Phys. Commun.* **2010**, *181*, 1477-1489.
- (9) Oskam, G.; Bergeron, B. V.; Meyer, G. J.; Searson, P. C. Pseudohalogens for dye-sensitized TiO₂ photoelectrochemical cells. *J. Phys. Chem. B* **2001**, *105*, 6867-6873.
- (10) Mayo, S. L.; Olafson, B. D.; Goddard, W. A. DREIDING - A GENERIC FORCE-FIELD FOR MOLECULAR SIMULATIONS. *J. Phys. Chem.* **1990**, *94*, 8897-8909.
- (11) Alimohammadi, M.; Fichthorn, K. A. A Force Field for the Interaction of Water with TiO₂ Surfaces. *J. Phys. Chem. C* **2011**, *115*, 24206-24214.
- (12) Tan, B.; Wu, Y. Y. Dye-sensitized solar cells based on anatase TiO₂ nanoparticle/nanowire composites. *J. Phys. Chem. B* **2006**, *110*, 15932-15938.
- (13) Pijpers, J. J. H.; Ulbricht, R.; Derossi, S.; Reek, J. N. H.; Bonn, M. Picosecond Electron Injection Dynamics in Dye-Sensitized Oxides in the Presence of Electrolyte. *J. Phys. Chem. C* **2011**, *115*, 2578-2584.
- (14) Nazeeruddin, M. K.; Humphry-Baker, R.; Liska, P.; Gratzel, M. Investigation of sensitizer adsorption and the influence of protons on current and voltage of a dye-sensitized nanocrystalline TiO₂ solar cell. *J. Phys. Chem. B* **2003**, *107*, 8981-8987.
- (15) Johansson, E. M. J.; Hedlund, M.; Siegbahn, H.; Rensmo, H. Electronic and molecular surface structure of Ru(tcterpy)(NCS)(3) and Ru(dcbpy)(2)(NCS)(2) adsorbed from solution onto nanostructured TiO₂: A photoelectron spectroscopy study. *J. Phys. Chem. B* **2005**, *109*, 22256-22263.
- (16) Nazeeruddin, M. K.; Zakeeruddin, S. M.; Humphry-Baker, R.; Jirousek, M.; Liska, P.; Vlachopoulos, N.; Shklover, V.; Fischer, C. H.; Gratzel, M. Acid-base equilibria of (2,2'-bipyridyl-4,4'-dicarboxylic acid)ruthenium(II) complexes and the effect of protonation on charge-transfer sensitization of nanocrystalline titania. *Inorg. Chem.* **1999**, *38*, 6298-6305.
- (17) Rappe, A. K.; Casewit, C. J.; Colwell, K. S.; Goddard, W. A.; Skiff, W. M. UFF, A FULL PERIODIC-TABLE FORCE-FIELD FOR MOLECULAR MECHANICS AND MOLECULAR-DYNAMICS SIMULATIONS. *J. Am. Chem. Soc.* **1992**, *114*, 10024-10035.
- (18) Evans, D. J. M., G. P. Statistical Mechanics of Nonequilibrium Liquids. *Academic Press:London* **1990**.
- (19) Trzesniak, D.; Kunz, A. P. E.; van Gunsteren, W. F. A comparison of methods to compute the potential of mean force. *ChemPhysChem* **2007**, *8*, 162-169.